ACS APPLIED MATERIALS & INTERFACES

Research Article

www.acsami.org

Roll-to-Roll Nanomanufacturing of Hybrid Nanostructures for Energy Storage Device Design

Landon Oakes,[†,‡] Trevor Hanken,[‡] Rachel Carter,[‡] William Yates,[‡] and Cary L. Pint*[,†,‡]

[†]Interdisciplinary Materials Science and Engineering, Vanderbilt University, Nashville, Tennessee 37212, United States

[‡]Mechanical Engineering, Vanderbilt University, Nashville, Tennessee 37212, United States

Supporting Information

ABSTRACT: A key limitation to the practical incorporation of nanostructured materials into emerging applications is the challenge of achieving low-cost, high throughput, and highly replicable scalable nanomanufacturing techniques to produce functional materials. Here, we report a benchtop roll-to-roll technique that builds upon the use of binary solutions of nanomaterials and liquid electrophoretic assembly to rapidly construct hybrid materials for battery design applications. We demonstrate surfactant-free hybrid mixtures of carbon nanotubes, silicon nanoparticles, MoS_2 nanosheets, carbon nanohorns, and graphene nanoplatelets. Roll-to-roll electrophoretic assembly from these solutions enables the controlled fabrication of homogeneous coatings of these nanostructures that maintain chemical and physical properties defined by the synergistic combination of nanomaterials utilized without adverse effects of surfactants or impurities that typically limit liquid nanomanufacturing routes. To demonstrate the utility of this nanomanufacturing approach, we employed roll-to-roll electrophoretic processing to fabricate both positive and negative electrodes for lithium ion batteries in less than 30 s. The optimized full-cell battery, containing active materials of prelithiated silicon nanoparticles and MoS_2 nanosheets, was assessed to exhibit energy densities of 167 Wh/kgcell^{-1} and power densities of 9.6 kW/kgcell^{-1}.

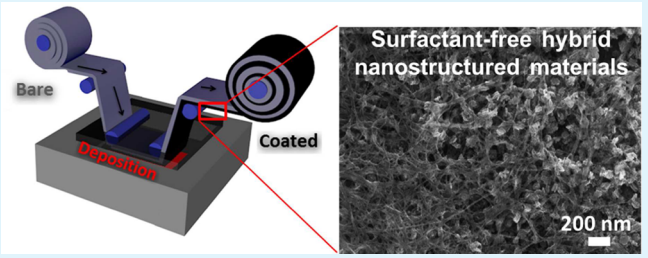

KEYWORDS: *roll-to-roll, nanomanufacturing, electrophoretic deposition, hybrid nanomaterials, silicon nanoparticles, MoS_2, carbon nanotubes, carbon nanohorns, graphene, lithium ion battery*

INTRODUCTION

Scalable manufacturing of nanomaterials is challenged by factors typically benign to conventional manufacturing routes for bulk materials.[1−3] Whereas nanostructures are consistently lauded for improved performance in applications at the laboratory scale, fabrication processes and costs for industrial processing often limit near-term commercial impact of many nanomaterial-based applications. Additionally, unlike bulk materials, the physical and chemical properties of materials composed of nanostructures are strongly correlated to impurities that interact with the nanostructures and the transport paths between adjacent nanoscale building blocks in the material. This provides two extremes for nanomaterial fabrication: (i) highly precise, expensive fabrication routes carried out in clean environments (e.g., ultraviolet or electron-based lithographic techniques), or (ii) large-scale, low-cost "coarse" material processing that relies on the use of liquid processing with surfactants (e.g., colloidal processing such as blade coating and/or electrophoretic deposition (EPD)).[4−6] Our efforts aim to explore the medium existing between these two processing routes where scalability and control or precision can be simultaneously achieved.[7,8]

In recent years, EPD has specifically been demonstrated as a versatile tool in the laboratory-scale fabrication of nanomaterials for broad applications, spanning energy storage and conversion,[9,10] sensing,[11] and optical devices,[12] among others. EPD enables the formation of pinhole-free films conformally layered on arbitrary materials with characteristics such as controllable thickness, macroscopic uniformity, rapid formation rates, and uniquely high packing efficiencies.[13−16] Recent advances in the understanding of EPD processes have driven interest toward industry scale manufacturing of nanomaterials.[17−20] This is compounded by research efforts in recent years to couple 1D and 2D materials with EPD, such as graphene, carbon nanotubes, and nanoparticles[21−23] in addition to hybrids of these materials.[24−27] However, most techniques demonstrating EPD of these materials require the use of additives or surfactants, which leads to the retention of these impurities in the deposited material that inhibits physical and chemical performance. Recently, substantial progress has been made in solubilizing low-dimensional nanostructures in surfactant-free solutions through the use of highly polar solvents or superacids.[28−30] In this regard, 1-methyl-2-pyrrolidone (NMP) has demonstrated growing popularity for solution processing of individual carbon nanostructures as well as other 2-D materials[31−33] due to its exceptionally high surface

Received: February 10, 2015
Accepted: June 8, 2015
Published: June 8, 2015

DOI: 10.1021/acsami.5b01315
ACS Appl. Mater. Interfaces 2015, 7, 14201−14210

tension ($\gamma > 40$ mJ/m^2) and highly polar nature. The properties of this solution make it amenable to both solubilization of SWCNTs and exfoliation of transition metal dichalcogenides (TMD) enabling one-batch processing of SWCNTs and exfoliated hybrid materials. Our recent work has demonstrated EPD of nanostructures from these polar solvent dispersions, enabling clean and pristine nanostructure deposition on a variety of substrates.[15,34,35]

EPD has specifically been demonstrated as a versatile tool for the preparation of energy storage device electrodes, including supercapacitors, pseudocapacitors, and battery anodes.[17,35−39] Significant research has been carried out to study the performance of various materials as anodes for lithium ion batteries, with silicon being distinguished for its ability to maintain high capacities (10X greater than conventional carbon anodes[40−42]). Alternatively, transition metals are conventionally used as cathodes, due to the ability to achieve high voltage when paired with graphite anodes and inhibit degradation under Li^+ oxidation and reduction reactions. However, a challenge for innovation in battery research is to not isolate the performance of a single component (anode, cathode, or electrolyte) of a battery, but instead to harness the versatility to engineer all working components simultaneously and thus engineer the performance of *full-cells*.[43] This requires versatility in the materials processing approach that goes beyond applications-based assessment of individual materials using a discovery-driven approach, and can leverage rational design of materials with high throughput for next-generation energy storage systems.

Therefore, in this work, we overcome these challenges by demonstrating the operation of a benchtop roll-to-roll platform to produce high-throughput, clean coatings of hybrid materials that can facilitate battery design applications. To demonstrate this approach, we focus specifically on hybrid materials composed of single-walled carbon nanotubes (SWCNTs) combined with graphene nanoplatelets, MoS_2 nanosheets, silicon nanoparticles, and single-walled carbon nanohorns (SWCNH). We demonstrate EPD from polar solvent solutions containing mixtures of these nanostructures in order to form homogeneous coatings that are comprised of hybrid nanostructured materials. These coatings are then assessed for their composition-dependent lithium reduction/oxidation energetics, which leads us to a full-cell battery design with electrodes produced in under 30 s with an optimized design that incorporates silicon nanoparticles as an anode (prelithiated), and MoS_2 nanosheets as a cathode. This device is assessed in a full-cell configuration and is found to exhibit energy densities of 167 Wh/kgcell^{-1} and power densities of 9.6 kW/kgcell^{-1}.

EXPERIMENTAL SECTION

Preparation of Nanostructure Dispersions. For SWCNT materials, a solution of 0.5 mg/mL HiPco SWCNTs (Unidym, purified) dispersed in 1-methyl-2-pyrolidinone (Aldrich, 99.5%) was prepared and left to sit overnight. For hybrid materials, a starting solution of 0.5 mg/mL SWCNT in NMP was mixed with the other carbon nanomaterials, namely, single-walled carbon nanohorns,[15,44−46] carbon nanosheets (grade 4, cheaptubes), and carbonized silicon nanoparticles (U.S. Research Nanomaterials, Inc.) at a concentration of 0.5 mg/mL and left to sit overnight. To fabricate the MoS_2 hybrid solution used in this work, 20 mg of bulk MoS_2 powder (Aldrich, 99%) was mixed into 40 mL NMP and ultrasonicated for 12 h to achieve exfoliation, then, 20 mg of SWCNTs was added to the suspension, and the resulting solution was left to sit overnight. Prior to deposition all solutions were ultrasonicated for 1 h before placement into the roll-to-roll system's reservoir.

Electrophoretic Deposition of Hybrid Materials. Roll-to-roll (R2R) electrophoretic deposition of carbon-based nanomaterials was performed in a vertical EPD cell with a separation of 4 mm between a stainless steel counter electrode and the working electrode. For the fabrication of battery films a 316 stainless steel disc (Pred Materials) was mounted to a biased aluminum roller and rolled through the reservoir containing the depositing solution and stainless steel counter electrode under an applied bias of 500 V/cm using a 4 rpm gear motor (Servo City). For mass deposition studies, a 3 × 1.5 cm^2 aluminum strip of known mass was mounted to the roller using Teflon clips, mechanically moved into position above the counter electrode, and left to rest in this position under an applied bias of 100 V/cm for the specified time. To demonstrate continuous operation of the coating process, an aluminum roll of dimensions 1 m × 1.5 cm was mounted to either end of the system and continuously moved through solution at a rate of ∼1.5 cm/s under an applied electric field of 500 V/cm. Monitoring of current and the application of voltage was performed using a LabView-operated Keithley 2602A Sourcemeter. In all cases, depositions were parametrized with rolling speed as a fixed parameter, and voltage and deposition time as variable parameters, with the requirement that the total mass of a deposited film could be assessed accurately on an electrode small enough to fit into a coin cell battery testing assembly.

For layering deposition studies, a 3 × 1.5 cm^2 aluminum strip was coated with a hybrid solution under an applied electric field of 100 V/cm for 240 s. The coated strip was then left to dry overnight before returning to the bath for an additional coating under identical parameters. To ensure no redissolution of the SWCNTs was occurring during the EPD process, an aluminum strip was coated with SWCNTs using an applied bias of 100 V/cm for 240 s and left to dry overnight. Then, the reservoir was filled with a pristine solution of NMP and identical deposition parameters were carried out. The electrode was left to dry overnight and then the mass of SWCNTs before and after was compared.

Roll-to-Roll System Design. The roll-to-roll system was assembled by mounting gear motors (4 rpm, Servo City), powered by a 12 V, 2.5 A power supply (Servo City), onto a custom designed Teflon reservoir. The Teflon reservoir contained a 9 × 2 cm^2 well across which two Teflon rollers were mounted and at the bottom of which a 6 × 2 cm^2 steel plate was mounted. The roll was composed of a 1 cm × 1 m aluminum strip (Grainger) mounted on both ends to either gear motor. Electrical contact was made to the aluminum roll through a stationary wire brush and contact with the steel counter electrode was achieved using a custom fabricated electrical feedthrough. Potential was applied to the system using a Keithley 2400 Sourcemeter which also served to record the current passed.

Silicon Nanoparticle Carbon Passivation. Silicon nanoparticles with carbon surface passivation layers were prepared by placing crystalline silicon nanoparticles in a home-built chemical vapor deposition system using a Lindberg Blue 1″ quartz tube furnace. To achieve carbonization, atmospheric pressure chemical vapor deposition was carried out under a flow rate of 100 sccm Argon and 20 sccm Hydrogen gas (AL Compressed gas). The furnace was then heated to 650 °C at a ramp rate of 70 °C/min and the particles were annealed at that temperature for 10 min. After annealing, a flow rate of 1 sccm C_2H_2 was introduced and the furnace temperature ramped to 750 °C. Under these conditions, the particles were held at 750 °C for 30 min before ramping the temperature to 850 °C and held for 30 min followed by a final ramp to 900 °C. After 10 min at 900 °C, the C_2H_2 flow was shut off and the furnace cooled to room temperature under a flow of 100 sccm Argon and 20 sccm Hydrogen. This treatment was observed to leave the surface of the silicon nanoparticles coated by a conformal layer of carbon material, as discussed in previous work.[47]

Battery Fabrication and Testing. After film deposition the battery electrodes were dismounted from the system and left to dry horizontally overnight on glass slides covered by a Kimwipe. After drying, materials were weighed and then assembled into a coin cell utilizing a half-cell configuration with a lithium metal foil counter

DOI: 10.1021/acsami.5b01315
ACS Appl. Mater. Interfaces 2015, 7, 14201−14210

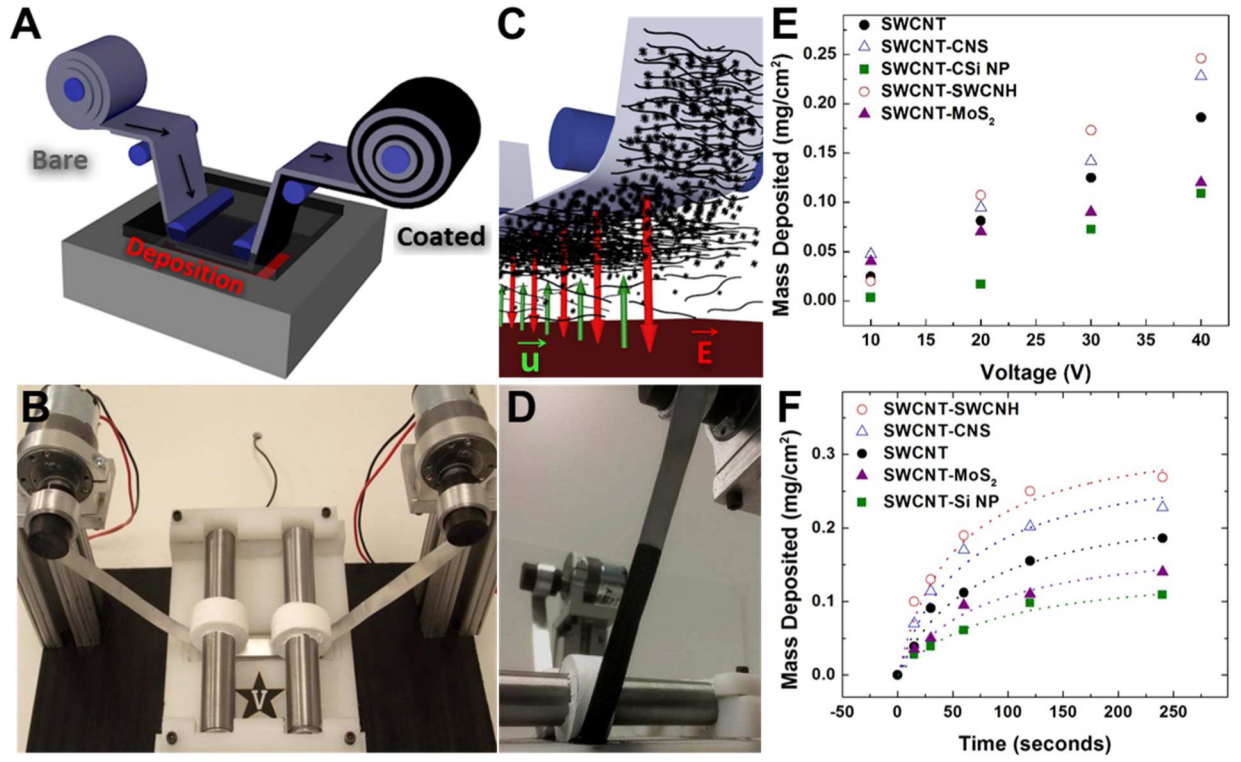

Figure 1. (A) Schematic of the roll-to-roll system used in this study and (B) the functional system used in this study. (C) Schematic demonstrating the EPD process within the system's reservoir and (D) an example of a coated roll generated with this process. (E) Mass deposited using this system as a function of applied voltage during a 240 s exposure time and (F) mass deposited as a function of deposition time for all hybrid materials studied. The dotted lines represent fits to the deposition generated from eq 4.

electrode, a 1 M $LiPF_6$ ethylene carbonate/dimethyl carbonate (Sigma–Aldrich) electrolyte solution and a Celgard battery separator. Assembly was performed in an argon-filled glovebox with O_2 levels <0.5 ppm (MBraun). Electrochemical testing was performed using a Metrohm Autolab multichannel testing system which performed both cyclic voltammetry and galvanostatic charge–discharge measurements.

Pre-Lithiation of Silicon Nanoparticle Composite. To achieve prelithiated SWCNT–Si NP composite materials, a 1 M $LiPF_6$ ethylene carbonate/diethyl carbonate (Sigma–Aldrich) electrolyte solution was drop cast in a thin layer atop a strip of lithium foil. The SWCNT–Si NP composite was placed directly on top of the lithium foil and pressure was applied through the use of a split test cell (MTI). The material was lithiated for 2 h and then placed directly in a coin cell with a SWCNT–MoS_2 cathode.

Material Characterization. Raman analysis was performed using a Renishaw inVia Raman microscope with a 532 nm excitation. Zetasizer measurements were carried out using a Malvern Zetasizer Nano ZS instrument.

RESULTS AND DISCUSSION

Underlying the ability to produce scalable coatings of pristine, hybrid nanostructures is the necessity to develop a platform that overcomes the "beaker-scale" processing limitations of most materials processing approaches. In order to achieve this, we developed a fully automated, benchtop R2R system that builds upon the widely known process of electrophoretic deposition in the framework of industrial-scale roll-to-roll process design. The operating principle of this system (Figure 1A) utilizes a roll of material (with a composition that can vary across a wide range of conductive foils and substrates[15,48]), that is rolled through a pool of solution, coated in a controllable manner, and then collected in a roll on the opposing side. When the foil is submerged in the liquid, an electric field is applied between the top and bottom electrodes to generate a constant electric field, despite the continuous movement of the top foil electrode. This transforms a conventional "beaker-scale" EPD process into a scalable platform that we demonstrate is an effective tool for nanomanufacturing. A photograph of the benchtop R2R system developed for this study is presented in Figure 1B, with an empty liquid reservoir for the purposes of visualization. This system was constructed and operated with cost of parts and equipment totaling under $300. Overall, this system is a critical feature that enables the rapid, large-area coating of clean, functional, and hybrid nanomaterials yielding the capability to produce full-cell battery electrodes in less than 60 s and perform rapid assessment of complex nanomaterial electrodes for practical battery design.

Coatings of various dispersed nanomaterials were fabricated with this system by applying an electric field of 100 V/cm between a stainless steel counter electrode (immersed in solution) and an aluminum foil roll that is extended between the two rollers (a complete discussion of the R2R EPD parameters is presented in the Experimental Section). A coated foil showing the clear demarcation point when the voltage is turned "on" and a scheme of the deposition process are shown in Figure 1, parts C and D. In this system design, faster deposition rates per unit electrode area can be achieved both by increasing the electric field intensity or decreasing the rolling rate of the electrode. This is generally illustrated in Figure 1, parts E and 1F, where deposited mass of coatings containing SWCNTs or hybrid coatings of SWCNTs combined with carbon nanosheets (CNS), silicon nanoparticles (Si NP), single-walled carbon nanohorns (SWCNHS), and exfoliated MoS_2 nanosheets is demonstrated as a function of absolute voltage and total deposition time. This is the basis for

DOI: 10.1021/acsami.5b01315
ACS Appl. Mater. Interfaces 2015, 7, 14201–14210

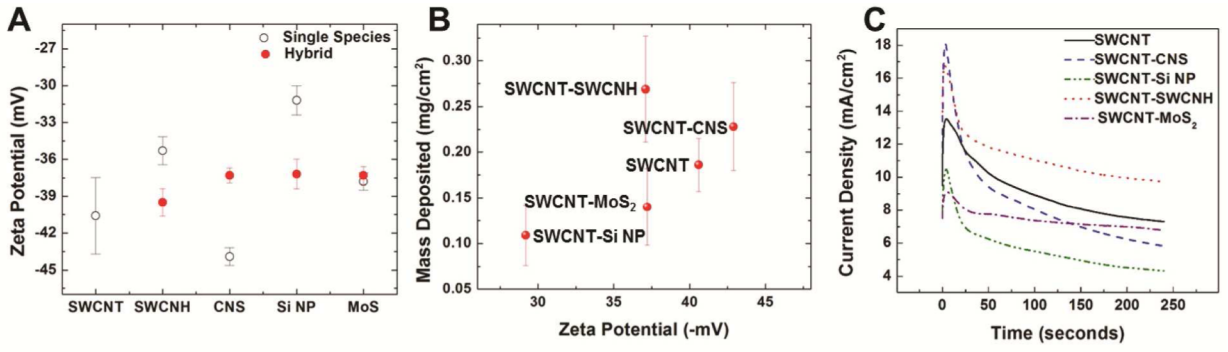

Figure 2. (A) Measurement of the zeta potential for individual nanomaterial species (open circles) and hybridized nanomaterials (closed circles) averaged over 3 measurements (B) Mass deposited as a function cosuspended nanomaterials averaged over 5 depositions and (C) current density during 240 s depositions.

parametrization of the system to achieve coatings that can be assessed for battery performance. From Figure 1E, the mass deposited is observed to exhibit a nearly linear relationship with the applied voltage in all cases. Figure 1F indicates further that the total mass deposited is a nonlinear function of the total deposition time. The dotted lines in the figure represent fits to the data using a model that is discussed at length at a later point. Notably, the capability to engineer deposition process parameters by decoupling deposition time and voltage is unique to a continuous process and cannot be achieved in conventional "beaker-scale" EPD processes straightforwardly, where a static process couples all experimental parameters into a single experimental output. Due to its polar nature, NMP has been demonstrated as an excellent solvent for native dispersion and/or exfoliation of nanostructured materials, many of which can only otherwise be suspended using surfactant solutions. Our recent efforts have demonstrated that EPD of SWCNTs from NMP polar solvents yields materials where electrochemical and thermogravimetric analysis confirms the pristine quality of the coatings, in comparison to processes carried out with surfactants that yield a significant (up to 50% by weight) mass due to impurities.[34] As the basis of EPD processing of nanomaterials has previously been built on surfactant or ion additive-enabled processes, our approach not only enables R2R capability, but simultaneously leads to an impurity-free coating process, which is critical toward the performance of nanostructured materials. As the basis of hybrid nanomaterial development rests on the cooperative function of different nanostructures, the use of surfactants or additives can compromise the benefits of a hybrid material.[34,35] Overall, the R2R EPD process builds a foundation for high throughput material fabrication that can enable avenues for rapid design and assessment of complex, functional nanostructured materials that can be tedious and challenging to develop with other top-down fabrication approaches.

One of the most critical parameters for EPD processing is the zeta potential, which is a general representation of the net charge on a particle dispersed in a solution. For EPD processing, the rate at which a particle moves to an electrode under an applied electric field is noted as the electrophoretic mobility represented below by the Smoluchowski approximation:

$$\mu = \frac{E\varepsilon\varepsilon_0\zeta}{\eta} \tag{1}$$

For ε the dielectric constant of the liquid, ε_0 the permittivity of free space, ζ the zeta potential of the particles, η the viscosity of the liquid, and E the applied electric field. For solutions with NMP, dispersed nanomaterials acquire a net negative charge through electron transfer reactions with the solvent molecules[49] (Figure 2A) and are subsequently attracted to the anode in an EPD process resulting in film formation (Supporting Information, SI, Figure S1A,B). Notably, for hybridized solutions of nanostructures, the zeta potential values represent a weighted average of the individual species. In all cases, the rate of deposition is strongly dependent on the degree of electrostatic stabilization within solution, and a strong correlation is observed between the limiting mass deposition rate and the zeta potential of the cosuspended particles (Figure 2B). While deposition rates vary with solution composition, uniform film formation and an exponentially decaying mass deposition rate is observed across all systems. Insights into this effect are obtained through in situ monitoring of the applied current during the EPD process (Figure 2C). This indicates that due to the high aspect ratio of SWCNTs, the growing concentration of SWCNTs at the electrode surface locally increases the viscosity of the solution in the vicinity of the electrode thereby inhibiting migration as the electrophoretic mobility has an inverse relationship with solution viscosity.[50,51] To investigate this effect, simulations were performed using a model similar to that developed by Sarkar et al. to simulate constant voltage depositions.[48] In constant-voltage EPD a variable mobility parameter, $\mu(t)$, is implemented to account for changes in particle mobility that arise from screening of the applied electric field by the growing, insulating deposit:

$$\int \mathrm{d}W = f \iint \mathrm{d}S\mu(t)C(t)\,\mathrm{d}t \tag{2}$$

where a weight dW is deposited on an area dS of the electrode. In this case, f represents the "sticking factor" which varies between the different nanostructures, $\mu(t)$ the particle velocity, and $C(t)$ the solution concentration. In the case of EPD of SWCNTs, however, it was found that the changes in particle mobility may be attributed to the drastic increase in solution viscosity near the vicinity of the electrode. SWCNTs represent a material which exhibits a significant concentration-dependent relationship with solution viscosity.[52−54] Due to the proposed "entanglement effect", viscosity changes within solution scale nonlinearly with CNT concentration yielding dramatic changes over multiple orders of magnitude when CNTs comprise a significant fraction of the solution volume. In EPD, the imposed

DOI: 10.1021/acsami.5b01315
ACS Appl. Mater. Interfaces 2015, 7, 14201−14210

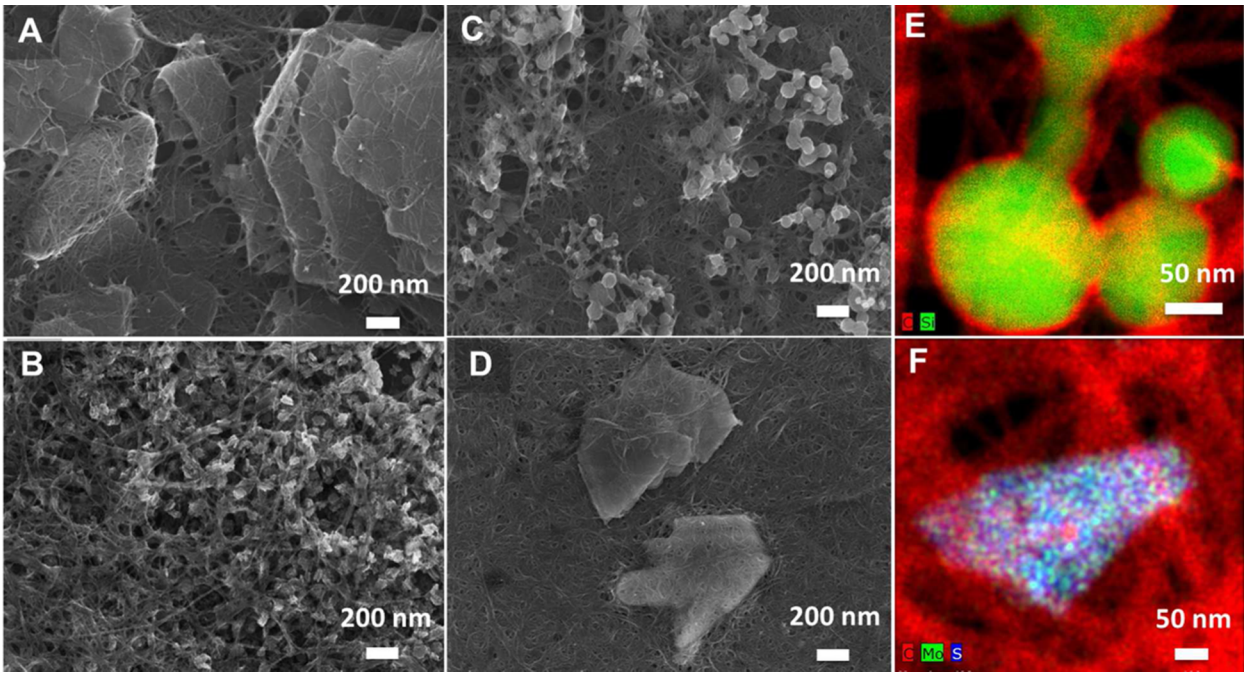

Figure 3. SEM images of deposited films on the stainless steel current collector for the various nanomaterials: (A) SWCNT−CNS, (B) SWCNT−SWCNH, (C) SWCNT−Si NP, and (D) SWCNT−MoS_2 NPs. Elemental mapping was performed using EDS TEM analysis to emphasize (E) the carbon coating for the silicon nanoparticles and (F) the presence of MoS_2 nanosheets. Notably, in EDS images, carbon is colored red, sulfur is colored blue, and green corresponds to silicon in 1E and molybdenum in 1F, respectively.

migration of SWCNTs creates a significant concentration of SWCNTs in the vicinity of the electrode thereby substantially influencing the viscosity. Therefore, simulations were performed using a time-dependent viscosity parameter. A plot of the calculated viscosity during the deposition is provided in SI Figure S2. Changes in particle mobility were accounted for by substituting a time-dependent viscosity parameter into eq 1. Notably, the effects of film formation on changes in the applied field were neglected, as the CNTs themselves form a conducting layer with similar conductivity as the electrode itself.[55] Thus, the following equation for EPD of SWCNTs was obtained by substitution of the time-dependent viscosity parameter into eq 1:

$$\int \mathrm{d}W = fE \iint \mathrm{d}S \frac{\varepsilon_0 \varepsilon \zeta}{\eta(t)} C(t)\, \mathrm{d}t \tag{3}$$

For hybrid materials, the total mass deposited is the sum of the deposition of SWCNTs and the cosuspended material:

$$\int \mathrm{d}W = fE \iint \mathrm{d}S \frac{\varepsilon_0 \varepsilon \zeta_{\mathrm{CNT}}}{\eta(t)} C_{\mathrm{CNT}}(t)\, \mathrm{d}t + fE \iint \mathrm{d}S \frac{\varepsilon_0 \varepsilon \zeta_{\text{co-particle}}}{\eta(t)} C_{\text{co-particle}}(t)\, \mathrm{d}t \tag{4}$$

where ζ_{CNT} and $C_{\mathrm{CNT}}(t)$ represent the zeta potential and concentration of SWCNTs, respectively, and $\zeta_{\text{co-particle}}$ and $C_{\text{co-particle}}(t)$ represent the zeta potential and concentrations for the cosuspended nanomaterials. An extended discussion of these calculations is presented in the SI.

In all cases, we utilize hybridized solutions of nanostructures to yield coatings containing hybrid nanomaterials. This builds upon the notion that a polar solvent will screen excessive particle−particle interaction between dissimilar species, and hence EPD processing will lead to homogeneous coatings of hybrid materials. Overall, we observe this to be the case, with representative images of the hybrid materials formed in this process shown in Figure 3. Whereas numerous combinations of these different nanostructures could be studied, we chose SWCNTs to be a common component between all hybrid materials due to the web-like nature of the SWCNTs that can empower a hybrid material with improved electrical and mechanical connectivity between the nanostructures. Figure 3, parts A−D, shows SEM images showing representative homogeneous coatings of SWCNT−CNS, SWCNT−SWCNH, SWCNT−Si NP, and SWCNT−MoS_2 hybrid materials, respectively. Furthermore, the chemical identity of the SWCNT−Si NP and SWCNT−MoS_2 species are identified through energy dispersive X-ray maps taken in the transmission electron microscope (TEM) in Figure 3, parts E and F. Notably, prior to dispersion of the Si NPs, we utilize a chemical vapor deposition process to catalytically stabilize the surface of the Si with a thin carbon layer, evident in Figure 3E as a thin red shell around the Si core. This is important not only for silicon chemical stability in EPD processing, but also for stability in electrochemical devices,[56] Overall, we observe that the nature of the intense electric field confined within the diffuse electrostatic boundary layer near the electrode surface provides a natural leveling mechanism capable of giving rise to exceptionally uniform film density and coverage on regions of the electrode not disturbed by other steps in the processing (SI Figure S3). Drying effects, electrode surface roughness, and movement in and out of solution may often induce clumping effects (e.g., SI Figure S1B), however, initial film formation is shown to be a highly uniform process.[57]

To investigate the ability of this process to produce layered materials, electrodes were coated with subsequent layers of SWCNTs and hybrid nanomaterials to investigate the effect of the SWCNT film on the EPD process. Deposited SWCNTs were left to dry overnight on the deposition electrode before

DOI: 10.1021/acsami.5b01315
ACS Appl. Mater. Interfaces 2015, 7, 14201−14210

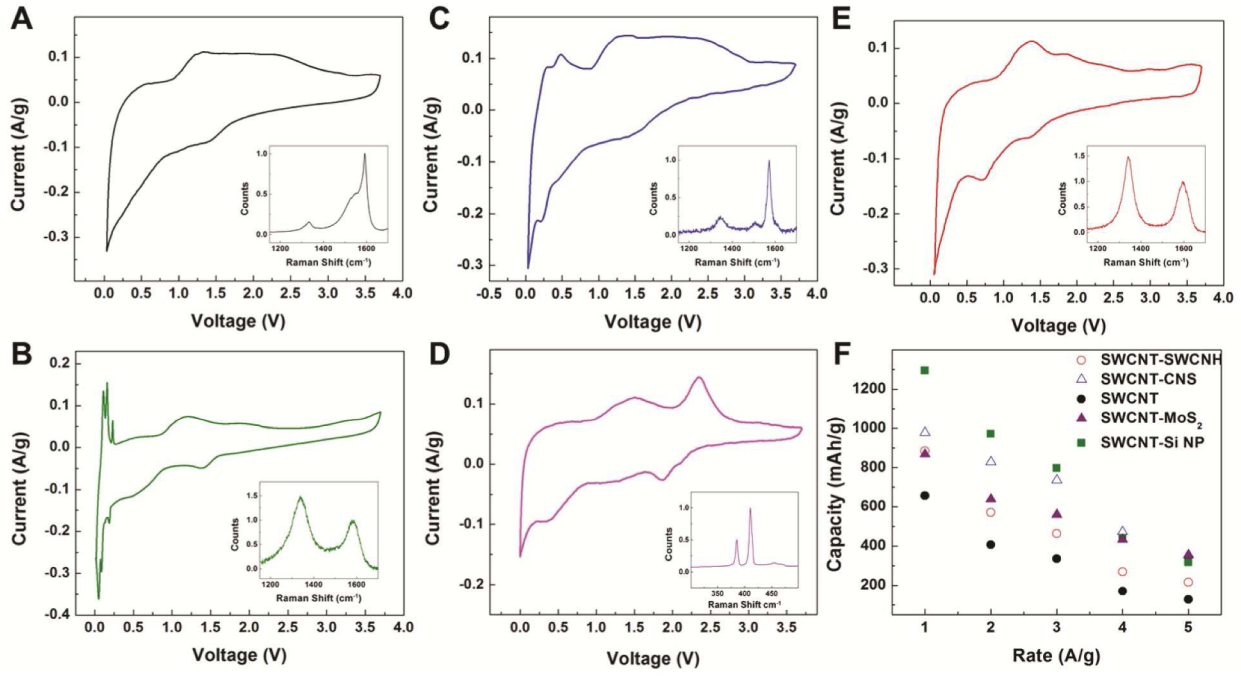

Figure 4. CV scans performed at 0.1 mV/s for (A) SWCNT, (B) SWCNT−Si NPs, (C) SWCNT−CNS, (D) SWCNT−MoS_2 NPs, and (E) SWCNT−SWCNHs, and (F) galvanostatic charge-discharge rate study for the hybrid nanomaterials, with sectioned curves for 1F available in the SI.

returning to the EPD bath for an additional coating. To ensure any changes in mass were not due to the delamination of the SWCNT coating in the solvent, a "dry run" was performed to investigate the amount of material lost due to redissolution of the SWCNT film. For this study, an SWCNT-coated electrode was placed into a bath of pure NMP under identical EPD conditions and a comparison of the mass before and after demonstrated that the SWCNT coating does not redissolve in the NMP (SI Figure S4a). Additionally, by coating a second layer of active material onto the precoated electrodes, it was found that nearly identical deposition rates were obtained for precoated electrodes (SI Figure S4b) compared with uncoated electrodes, further emphasizing the fact that the decay in deposition rate over time is a direct consequence of solution properties near the electrode surface and not due to resistance in the growing film. Additionally, this provides a mechanism to allow for coating of multiple subsequent layers of nanomaterials, which could potentially even be accomplished in adjacent solution baths in the same R2R system, with advanced capability to nanomanufacture controlled architectures such as gradients and patterned films.

While results from the lab-scale benchtop R2R system developed here seem promising, a number of considerations must be made when scaling such a system to manufacturing scales. First, continual depletion of the depositing material can result in a changing concentration of active species within the deposition reservoir leading to potentially variable mass deposition rates. Second, studies have shown through finite element analysis that for short deposition times and thin EPD films, a buildup of material can occur on the edges of the electrode causing nonuniformities within the deposited films.[58] Our effort used the entire deposited electrode to fabricate the battery electrode and thus did not observe such nonuniformities; however, if electrodes were made from different sections of the same deposition electrode, this is an effect that should be considered.

One of the key application areas where such nanomanufacturing routes could prove valuable is in the fabrication and optimization of battery materials. Conventional approaches to analyzing the oxidation and reduction energetics of Faradaic energy storage reactions often distinguish materials only by the chemical composition (e.g., carbon, silicon, etc.) and not by the nanostructured characteristics of the material. Furthermore, the challenge in any battery-focused effort, especially in lithium-ion or other metal-ion batteries, is the development of a full-cell architecture that involves optimized anode, cathode, and electrolyte combinations. This is challenging due to the codependence of both electrode chemical stability and metal ion storage potential of each individual component on the combination that is chosen. Our focus for the remainder of this report is to demonstrate an effort whereby the high throughput R2R system discussed above enables a rational approach to battery design by overcoming both of these challenges and producing an operational full-cell battery from nanomanufactured hybrid nanomaterials produced in this study.

The first step in this process is to assess the energetics of Faradaic chemical reactions occurring between the hybrid materials produced in this R2R technique and half-cell configurations. To accomplish this, cyclic voltammetry (CV) scans at a rate of 0.1 mV/s were performed in half cell configurations (vs Li electrodes), and the results are summarized in Figure 4. The electrodes were consistent with previously described materials, and were produced in as little as 30 s using this R2R nanomanufacturing technique. For each CV curve, representative Raman spectra of the hybrid material is presented as an inset. CV analysis of the SWCNT film emphasizes that a majority of the Faradaic charge-transfer reactions arising from storage on the SWCNT surface lies in a broad Faradaic storage peak between ∼1−3 V vs Li/Li^+. For our system, this storage regime gives rise to a capacity of 658 mAh/g. Density functional theory calculations have emphasized that these reactions may be mediated through surface defective

DOI: 10.1021/acsami.5b01315
ACS Appl. Mater. Interfaces 2015, 7, 14201−14210

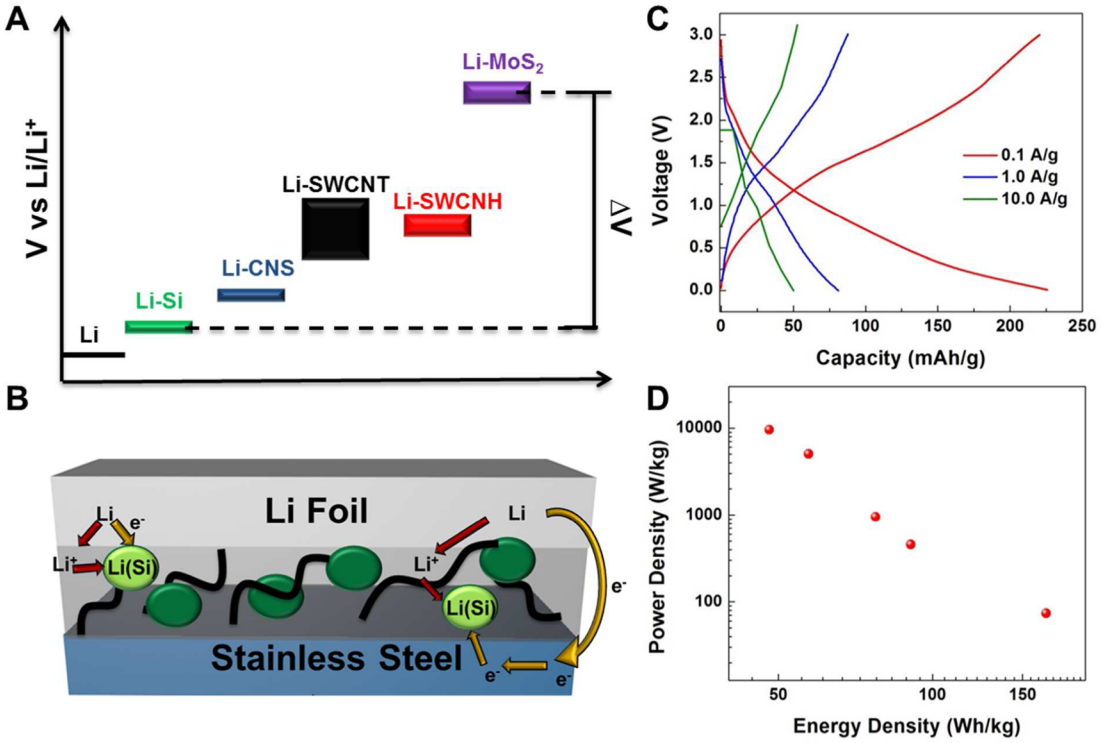

Figure 5. (A) Schematic illustration of the wide range of potentials capable of Faradaic lithiation reactions for the different nanostructures investigated. (B) Schematic illustration of the prelithiation process in Si NP−SWCNT films. (C) Charge−discharge characteristics of the full cell device fabricated with a prelithiated SWCNT−Si NP anode and SWCNT−MoS_2 NS cathode. (D) Ragone analysis of the full cell device.

carbon sites,[59] as these do not occur in the same potential window as intercalation in graphite. Hybrid SWCNT−SWCNH materials, which exhibit an exceptionally high defect density, yield substantial enhancement to charge stored in this regime as observed through higher peak current values during CV scans as well as greater capacities during device cycling yielding a maximum capacity of 884 mAh/g. For CNS, a material with low defect density, little-to-no enhancement in this regime is observed; however, an additional capacity is provided at lower potentials through the intercalation of lithium between graphitic sheets yielding an improved capacity of 978 mAh/g. For SWCNT−Si NP hybrids, whereas there is some indication of carbon storage that we chiefly attribute to the SWCNT hybrid material, exceptional capacity is observed in the low-voltage lithiation reactions in silicon. This is evident from the large peak currents observed in Figure 4D at low voltages vs Li/Li^+ and a maximum capacity of 1294 mAh/g for this electrode material. By producing SWCNT−MoS_2 NS hybrid materials (Figure 4E), energy storage at high potentials was achieved due to the Li_2S storage mechanism previously defined for MoS_2 NSs yielding capacities as high as 867 mAh/g. The capacities of the hybrid materials, as measured from Galvanostatic charge−discharge measurements, are presented in Figure 4F as a function of the total rate relative to the total hybrid electrode material mass. Representative charge−discharge curves for all materials are presented in SI Figure S5. Additionally, we have performed error analysis on the measured SWCNT electrode devices to assess the sample-to-sample variation in electrochemical performance. This is presented in the SI (Figure S6).

As is evident in Figure 4, the energetics for lithium insertion and removal can be tuned across the spectrum of the stability window of the electrolyte by using these different electrode materials. In all cases, these reduction and oxidation potentials, which are evident in CV scans, are measured against a lithium electrode. Since the use of pure lithium electrodes in full cell architectures leads to dendrite formation,[60,61] a key challenge for constructing a full-cell battery is to maintain $a > 1.5$ V potential difference between redox potentials of either electrode (fixed by technological requirements, which are based on conventional alkaline batteries), while utilizing the same electrolyte. To accomplish this, we utilize information obtained from CV analysis to generate a diagram of observed redox potentials (Figure 5A), which is inferred from CV scans. In this case, the redox potential for the MoS_2 hybrid material is the highest due to Faradaic storage processes between Li and S species. The higher potential of this system makes MoS_2 a candidate for use as the cathode material in a full-cell architecture. Conversely, aside from lithium metal, the Si NPs exhibit a redox potential that is the lowest of those studied in this work. Therefore, Si NPs are a practical choice for an anode material in a full-cell architecture (Figure 5A). As Si NPs do not natively contain Li species, lithiation was achieved for anodes in a full cell configuration by placing the SWCNT−Si NP electrode materials in direct contact with lithium foil for 3 h (Figure 5B). As previously reported, silicon in direct contact with lithium foil will form an Li−Si alloy providing a facile mechanism to fabricate a source for lithium ions during device cycling.[62] Compared to previous work by Liu et al.,[62] we demonstrate that this prelithiation can be achieved with carbon coated silicon nanoparticles, which in itself is a new observation. In order to characterize the performance of this device, we carried out Galvanostatic charge−discharge measurements at varying currents, with three representative curves for three currents of 100, 1, and 10 A/g (Figure 5C). Notably, at rates appropriate for conventional battery applications (100

DOI: 10.1021/acsami.5b01315
ACS Appl. Mater. Interfaces 2015, 7, 14201−14210

mA/g), we observed cell capacities of 225 mAh/g, which is comparable to conventional battery systems. However, the nanostructured characteristics of the electrodes, which enable rapid ion insertion from the electrolyte, still enable over 20% of this capacity to be accessed at 100X faster cycling rates, which is not achievable in full-cell battery systems with bulk electrodes. In order to further quantify the cell performance, we performed Ragone analysis to assess the energy-power characteristics of the device based on the total cell mass (Figure 5D). The energy density was calculated based on integration of the Galvanostatic voltage profiles, and power density was calculated as an average value based on the total energy released over the time duration of the discharge. A maximum energy density of 167 $Whkg_{cell}^{-1}$ was obtained corresponding to a capacity of 225 $mAhg_{cell}^{-1}$ when operated at 100 mAg_{cell}^{-1}. When operated at high charging currents of 10 Ag_{cell}^{-1}, power densities near 10 000 Wkg_{cell}^{-1} were measured, which is on par with the power capability of many modern day supercapacitors (Figure 5D), while still boasting energy densities near ∼40 $Whkg_{cell}^{-1}$. Whereas this performance is promising, the nanomanufacturing approach that underlies the ability to produce these electrodes is transferrable to many other applications, such as chemical sensing, optoelectronics, and energy conversion, where clean manufactured hybrid nanostructured materials could lead to improved or ideal performance in these platforms.

CONCLUSIONS

We demonstrate here the ability to utilize a low-cost (sub-$300), benchtop roll-to-roll system for the rapid development of nanomanufactured hybrid nanostructured materials. Our approach depends upon the utilization of surfactant-free NMP polar solvent solutions that both provide stable dispersions of hybrid nanostructure mixtures, and enable controllable EPD processing. Unlike conventional "beaker-scale" EPD routes, the roll-to-roll approach enables greater control over deposition parameters, empowers scalable processing conditions in a laboratory environment that intersects commercial applications, and provides the capability to assemble clean, functional hybrid materials that "bottom-up" fabrication routes are incapable of producing. We specifically demonstrate the fabrication of homogeneous hybrid nanostructured materials containing SWCNTs, SWCNHs, CNSs, Si NPs, and MoS_2 nanosheets, and demonstrate the application of these materials into electrodes for a full-cell lithium-ion battery design. Using electrodes that can be fabricated in as little as 30 s, we demonstrate an Si NP−MoS_2 all nanostructured material full cell battery that exhibits full cell capacities on par with conventional Li-ion batteries, but with improved power capability. As we envision the bottleneck for many commercial applications of nanomaterials to be low-cost, reliable, and scalable processing routes that build the foundation for product development and design, this nanomanufacturing approach, which seems unlimited in versatility in the choice of materials, brings potential for many applications extending beyond energy storage into areas of energy conversion, sensing, catalysis, optoelectronics, protective coatings, and other areas.

ASSOCIATED CONTENT

Supporting Information

Pictures of hybrid nanomaterial dispersions and deposited films from R2R system, cross-sectional SEM images, charge−discharge analysis of hybrid materials, cycling performance for full-cell nanomanufactured MoS_2-Si NP battery, data for layered nanostructure depositions, and considerations for error analysis of main text figures. The Supporting Information is available free of charge on the ACS Publications website at DOI: 10.1021/acsami.5b01315.

AUTHOR INFORMATION

Corresponding Author

*E-mail: cary.l.pint@vanderbilt.edu (C.L.P.).

Notes

The authors declare no competing financial interest.

ACKNOWLEDGMENTS

We thank D. Geohegan, C. Roleau, and A. Puretzky at ORNL for providing SWCNH materials utilized in this study. Additionally, we thank A. Westover, K. Share, and A. Cohn for discussions about the results of this work. This work was supported by NSF Nanomanufacturing award CMMI 1400424.

REFERENCES

(1) Vanli, O. A.; Rivero, I.; Wang, B. Advances in Nanomanufacturing: Process Repeatability, Scalability and Affordability for Nanomaterials and Manufacturing. *Int. J. Adv. Manuf. Technol.* **2013**, *64*, 513−514.

(2) Busnaina, A.; Mead, J.; Isaacs, J.; Somu, S. Nanomanufacturing and Sustainability: Opportunities and Challenges. *J. Nanopart. Res.* **2013**, *15*, 1−6.

(3) Wiesner, M. R.; Lowry, G. V.; Alvarez, P.; Dionysiou, D.; Biswas, P. Assessing the Risks of Manufactured Nanomaterials. *Environ. Sci. Technol.* **2006**, *40*, 4336−4345.

(4) Biswas, A.; Bayer, I. S.; Biris, A. S.; Wang, T.; Dervishi, E.; Faupel, F. Advances in Top−Down and Bottom−up Surface Nanofabrication: Techniques, Applications & Future Prospects. *Adv. Colloid Interface Sci.* **2012**, *170*, 2−27.

(5) Gates, B. D.; Xu, Q. B.; Stewart, M.; Ryan, D.; Willson, C. G.; Whitesides, G. M. New Approaches to Nanofabrication: Molding, Printing, and Other Techniques. *Chem. Rev.* **2005**, *105*, 1171−1196.

(6) Gajendran, P.; Devi, N. B.; Devasenathipathy, R. Recent Progress in Electrode Fabrication Materials and Various Insights in Solar Cells: Review. *Int. J. Electrochem. Sci.* **2015**, *10*, 3301−3318.

(7) de Villoria, R. G.; Hart, A. J.; Wardle, B. L. Continuous High-Yield Production of Vertically Aligned Carbon Nanotubes on 2D and 3D Substrates. *ACS Nano* **2011**, *5*, 4850−4857.

(8) Lee, M. H.; Lim, N.; Ruebusch, D. J.; Jamshidi, A.; Kapadia, R.; Lee, R.; Seok, T. J.; Takei, K.; Cho, K. Y.; Fan, Z.; Jang, H.; Wu, M.; Cho, G.; Javey, A. Roll-to-Roll Anodization and Etching of Aluminum Foils for High-Throughput Surface Nanotexturing. *Nano Lett.* **2011**, *11*, 3425−3430.

(9) Santhanagopalan, S.; Balram, A.; Meng, D. D. Scalable High-Power Redox Capacitors with Aligned Nanoforests of Crystalline MnO_2 Nanorods by High Voltage Electrophoretic Deposition. *ACS Nano* **2013**, *7*, 2114−2125.

(10) Brown, P.; Kamat, P. V. Quantum Dot Solar Cells. Electrophoretic Deposition of CdSe−C60 Composite Films and Capture of Photogenerated Electrons with N C60 Cluster Shell. *J. Am. Chem. Soc.* **2008**, *130*, 8890−8891.

(11) Subramanian, P.; Niedziolka-Jonsson, J.; Lesniewski, A.; Wang, Q.; Li, M.; Boukherroub, R.; Szunerits, S. Preparation of Reduced Graphene Oxide−Ni (OH) 2 Composites by Electrophoretic Deposition: Application for Non-Enzymatic Glucose Sensing. *J. Mater. Chem. A* **2014**, *2*, 5525−5533.

(12) Song, K. W.; Costi, R.; Bulović, V. Electrophoretic Deposition of CdSe/ZnS Quantum Dots for Light-Emitting Devices. *Adv. Mater.* **2013**, *25*, 1420−1423.

(13) Santhanagopalan, S.; Teng, F.; Meng, D. D. High-Voltage Electrophoretic Deposition for Vertically Aligned Forests of One-Dimensional Nanoparticles. *Langmuir* **2010**, *27*, 561−569.

DOI: 10.1021/acsami.5b01315
ACS Appl. Mater. Interfaces 2015, 7, 14201−14210

(14) Chávez-Valdez, A.; Boccaccini, A. R. Innovations in Electrophoretic Deposition: Alternating Current and Pulsed Direct Current Methods. *Electrochim. Acta* **2012**, *65*, 70−89.
(15) Oakes, L.; Westover, A.; Mahjouri-Samani, M.; Chatterjee, S.; Puretzky, A. A.; Rouleau, C.; Geohegan, D. B.; Pint, C. L. Uniform, Homogenous Coatings of Carbon Nanohorns on Arbitrary Substrates from Common Solvents. *ACS Appl. Mater. Interfaces* **2013**, *5*, 13153−13160.
(16) Brahma, N.; Talbot, J. B. Effects of CMP Slurry Additives on the Agglomeration of Alumina Nanoparticles 1: General Aggregation Rate Behavior. *J. Colloid Interface Sci.* **2014**, *419*, 56−60.
(17) Gonzalo-Juan, I.; Krejci, A.; Rodriguez, M.; Zhou, Y.; Fichthorn, K.; Dickerson, J. Dipole Moment-Tuned Packing of TiO_2 Nanocrystals into Monolayer Films by Electrophoretic Deposition. *Appl. Phys. Lett.* **2014**, *105*, 113108−1−113108−5.
(18) Pascall, A. J.; Qian, F.; Wang, G. M.; Worsley, M. A.; Li, Y.; Kuntz, J. D. Light-Directed Electrophoretic Deposition: A New Additive Manufacturing Technique for Arbitrarily Patterned 3D Composites. *Adv. Mater.* **2014**, *26*, 2252−2256.
(19) Kumar, A.; Kazmer, D. O.; Barry, C. M. F.; Mead, J. L. Pulsed Electric Field Assisted Assembly of Polyaniline. *Nanotechnology* **2012**, *23*, 335303−1−335303−10.
(20) Krejci, A. J.; Gebre, T.; Ruggiero, C. A.; Mochena, M. D.; Dickerson, J. H. Kinetics of Monolayer and Bilayer Nanoparticle Film Formation During Electrophoretic Deposition. *Adv. Appl.Ceram.* **2014**, *113*, 50−54.
(21) Krishnamurthy, S.; Kamat, P. V. CdSe−Graphene Oxide Light-Harvesting Assembly: Size-Dependent Electron Transfer and Light Energy Conversion Aspects. *ChemPhysChem* **2014**, *15*, 2129−2135.
(22) Golobostanfard, M. R.; Abdizadeh, H.; Mohajerzadeh, S. Incorporation of Carbon Nanotubes in a Hierarchical Porous Photoanode of Tandem Quantum Dot Sensitized Solar Cells. *Nanotechnology* **2014**, *25*, 345402.
(23) Chavez-Valdez, A.; Shaffer, M. S. P.; Boccaccini, A. R. Applications of Graphene Electrophoretic Deposition. A Review. *J. Phys. Chem. B* **2013**, *117*, 1502−1515.
(24) Zhu, G.; Pan, L.; Lu, T.; Xu, T.; Sun, Z. Electrophoretic Deposition of Reduced Graphene−Carbon Nanotubes Composite Films as Counter Electrodes of Dye-Sensitized Solar Cells. *J. Mater. Chem.* **2011**, *21*, 14869−14875.
(25) Yang, Y.; Chen, D.; Liu, B.; Zhao, J. Binder-Free Si Nanoparticle Electrode with 3-D Porous Structure Prepared by Electrophoretic Deposition for Lithium-Ion Batteries. *ACS Appl. Mater. Interfaces* **2015**, DOI: 10.1021/acsami.5b00421.
(26) Lin, J.-Y.; Chan, C.-Y.; Chou, S.-W. Electrophoretic Deposition of Transparent MoS_2−Graphene Nanosheet Composite Films as Counter Electrodes in Dye-Sensitized Solar Cells. *Chem. Commun.* **2013**, *49*, 1440−1442.
(27) Boccaccini, A.; Cho, J.; Subhani, T.; Kaya, C.; Kaya, F. Electrophoretic Deposition of Carbon Nanotube−Ceramic Nanocomposites. *J. Eur. Ceram. Soc.* **2010**, *30*, 1115−1129.
(28) Davis, V. A.; Parra-Vasquez, A. N. G.; Green, M. J.; Rai, P. K.; Behabtu, N.; Prieto, V.; Booker, R. D.; Schmidt, J.; Kesselman, E.; Zhou, W.; Fan, H.; Adams, W. W.; Hauge, R. H.; Fischer, J. E.; Cohen, Y.; Talmon, Y.; Smalley, R. E.; Pasquali, M. True Solutions of Single-Walled Carbon Nanotubes for Assembly into Macroscopic Materials. *Nat. Nanotechnol.* **2009**, *4*, 830−834.
(29) Behabtu, N.; Lomeda, J. R.; Green, M. J.; Higginbotham, A. L.; Sinitskii, A.; Kosynkin, D. V.; Tsentalovich, D.; Parra-Vasquez, A. N. G.; Schmidt, J.; Kesselman, E.; Cohen, Y.; Talmon, Y.; Tour, J. M.; Pasquali, M. Spontaneous High-Concentration Dispersions and Liquid Crystals of Graphene. *Nat. Nanotechnol.* **2010**, *5*, 406−411.
(30) Pirkle, A.; Chan, J.; Venugopal, A.; Hinojos, D.; Magnuson, C. W.; McDonnell, S.; Colombo, L.; Vogel, E. M.; Ruoff, R. S.; Wallace, R. M. The Effect of Chemical Residues on the Physical and Electrical Properties of Chemical Vapor Deposited Graphene Transferred to SiO_2. *Appl. Phys. Lett.* **2011**, *99*.
(31) Coleman, J. N.; Lotya, M.; O'Neill, A.; Bergin, S. D.; King, P. J.; Khan, U.; Young, K.; Gaucher, A.; De, S.; Smith, R. J.; Shvets, I. V.; Arora, S. K.; Stanton, G.; Kim, H. Y.; Lee, K.; Kim, G. T.; Duesberg, G. S.; Hallam, T.; Boland, J. J.; Wang, J. J.; Donegan, J. F.; Grunlan, J. C.; Moriarty, G.; Shmeliov, A.; Nicholls, R. J.; Perkins, J. M.; Grieveson, E. M.; Theuwissen, K.; McComb, D. W.; Nellist, P. D.; Nicolosi, V. Two-Dimensional Nanosheets Produced by Liquid Exfoliation of Layered Materials. *Science* **2011**, *331*, 568−571.
(32) Hu, Y. H.; Li, X. F.; Lushington, A.; Cai, M.; Geng, D. S.; Banis, M. N.; Li, R. Y.; Sun, X. L. Fabrication of MoS_2−Graphene Nanocomposites by Layer-by-Layer Manipulation for High-Performance Lithium Ion Battery Anodes. *ECS J. Solid State Sci. Technol.* **2013**, *2*, M3034−M3039.
(33) Cunningham, G.; Lotya, M.; Cucinotta, C. S.; Sanvito, S.; Bergin, S. D.; Menzel, R.; Shaffer, M. S. P.; Coleman, J. N. Solvent Exfoliation of Transition Metal Dichalcogenides: Dispersibility of Exfoliated Nanosheets Varies Only Weakly between Compounds. *ACS Nano* **2012**, *6*, 3468−3480.
(34) Carter, R.; Oakes, L.; Cohn, A. P.; Holzgrafe, J.; Zarick, H. F.; Chatterjee, S.; Bardhan, R.; Pint, C. L. Solution Assembled Single-Walled Carbon Nanotube Foams: Superior Performance in Supercapacitors, Lithium-Ion, and Lithium−Air Batteries. *J. Phys. Chem. C* **2014**, *118*, 20137−20151.
(35) Cohn, A. P.; Oakes, L.; Carter, R.; Chatterjee, S.; Westover, A. S.; Share, K.; Pint, C. L. Assessing the Improved Performance of Freestanding, Flexible Graphene and Carbon Nanotube Hybrid Foams for Lithium Ion Battery Anodes. *Nanoscale* **2014**, *6*, 4669−4675.
(36) Hwang, I. S.; Kim, J. C.; Seo, S. D.; Lee, S.; Lee, J. H.; Kim, D. W. A Binder-Free Ge-Nanoparticle Anode Assembled on Multiwalled Carbon Nanotube Networks for Li-Ion Batteries. *Chem. Commun.* **2012**, *48*, 7061−7063.
(37) Mazor, H.; Golodnitsky, D.; Burstein, L.; Gladkich, A.; Peled, E. Electrophoretic Deposition of Lithium Iron Phosphate Cathode for Thin-Film 3D-Microbatteries. *J. Power Sources* **2012**, *198*, 264−272.
(38) Ha, D. H.; Islam, M. A.; Robinson, R. D. Binder-Free and Carbon-Free Nanoparticle Batteries: A Method for Nanoparticle Electrodes without Polymeric Binders or Carbon Black. *Nano Lett.* **2012**, *12*, 5122−5130.
(39) Wang, M.; Duong, L. D.; Mai, N. T.; Kim, S.; Kim, Y.; Seo, H.; Kim, Y. C.; Jang, W.; Lee, Y.; Suhr, J.; Nam, J.-D. All-Solid-State Reduced Graphene Oxide Supercapacitor with Large Volumetric Capacitance and Ultralong Stability Prepared by Electrophoretic Deposition Method. *ACS Appl. Mater. Interfaces.* **2015**, *7* (2), 1348−1354.
(40) Chan, C. K.; Peng, H. L.; Liu, G.; McIlwrath, K.; Zhang, X. F.; Huggins, R. A.; Cui, Y. High-Performance Lithium Battery Anodes Using Silicon Nanowires. *Nat. Nanotechnol.* **2008**, *3*, 31−35.
(41) Yao, Y.; McDowell, M. T.; Ryu, I.; Wu, H.; Liu, N. A.; Hu, L. B.; Nix, W. D.; Cui, Y. Interconnected Silicon Hollow Nanospheres for Lithium-Ion Battery Anodes with Long Cycle Life. *Nano Lett.* **2011**, *11*, 2949−2954.
(42) Cui, L. F.; Yang, Y.; Hsu, C. M.; Cui, Y. Carbon−Silicon Core-Shell Nanowires as High Capacity Electrode for Lithium Ion Batteries. *Nano Lett.* **2009**, *9*, 3370−3374.
(43) Goodenough, J. B.; Park, K. S. The Li-Ion Rechargeable Battery: A Perspective. *J. Am. Chem. Soc.* **2013**, *135*, 1167−1176.
(44) Cheng, M. D.; Lee, D. W.; Zhao, B.; Hu, H.; Styers-Barnett, D. J.; Puretzky, A. A.; DePaoli, D. W.; Geohegan, D. B.; Ford, E. A.; Angelini, P. Formation Studies and Controlled Production of Carbon Nanohorns Using Continuous in Situ Characterization Techniques. *Nanotechnology.* **2007**, *18*, 185604.
(45) Chandrakumar, K. R. S.; Readle, J. D.; Rouleau, C.; Puretzky, A.; Geohegan, D. B.; More, K.; Krishnan, V.; Tian, M. K.; Duscher, G.; Sumpter, B.; Irle, S.; Morokuma, K. High- Temperature Transformation of Fe-Decorated Single-Wall Carbon Nanohorns to Nanooysters: A Combined Experimental and Theoretical Study. *Nanoscale* **2013**, *5*, 1849−1857.
(46) Puretzky, A. A.; Styers-Barnett, D. J.; Rouleau, C. M.; Hu, H.; Zhao, B.; Ivanov, I. N.; Geohegan, D. B. Cumulative and Continuous Laser Vaporization Synthesis of Single Wall Carbon Nanotubes and Nanohorns. *Appl. Phys. A: Mater. Sci. Process.* **2008**, *93*, 849−855.

DOI: 10.1021/acsami.5b01315
ACS Appl. Mater. Interfaces 2015, 7, 14201−14210

(47) Chatterjee, S.; Carter, R.; Oakes, L.; Erwin, W. R.; Bardhan, R.; Pint, C. L. Electrochemical and Corrosion Stability of Nanostructured Silicon by Graphene Coatings: Toward High Power Porous Silicon Supercapacitors. *J. Phys. Chem. C* **2014**, *118*, 10893−10902.
(48) Sarkar, P.; Nicholson, P. S. Electrophoretic Deposition (EPD): Mechanisms, Kinetics, and Application to Ceramics. *J. Am. Ceram. Soc.* **1996**, *79*, 1987−2002.
(49) Liu, W. W.; Wang, J. N.; Wang, X. X. Charging of Unfunctionalized Graphene in Organic Solvents. *Nanoscale* **2012**, *4*, 425−428.
(50) Grady, B. P. The Use of Solution Viscosity to Characterize Single-Walled Carbon Nanotube Dispersions. *Macromol. Chem. Phys.* **2006**, *207*, 2167−2169.
(51) Anné, G.; Neirinck, B.; Vanmeensel, K.; Biest, O.; Vleugels, J. Origin of the Potential Drop over the Deposit During Electrophoretic Deposition. *J. Am. Ceram. Soc.* **2006**, *89*, 823−828.
(52) Shaffer, M. S.; Fan, X.; Windle, A. Dispersion and Packing of Carbon Nanotubes. *Carbon* **1998**, *36*, 1603−1612.
(53) Halelfadl, S.; Estellé, P.; Aladag, B.; Doner, N.; Maré, T. Viscosity of Carbon Nanotubes Water-based Nanofluids: Influence of Concentration and Temperature. *Int. J. Therm. Sci.* **2013**, *71*, 111−117.
(54) Huang, Y. Y.; Terentjev, E. M. Dispersion of Carbon Nanotubes: Mixing, Sonication, Stabilization, and Composite Properties. *Polymers* **2012**, *4*, 275−295.
(55) Cho, J.; Konopka, K.; Rozniatowski, K.; Garcia-Lecina, E.; Shaffer, M. S. P.; Boccaccini, A. R. Characterisation of Carbon Nanotube Films Deposited by Electrophoretic Deposition. *Carbon* **2009**, *47*, 58−67.
(56) Ng, S. H.; Wang, J. Z.; Wexler, D.; Konstantinov, K.; Guo, Z. P.; Liu, H. K. Highly Reversible Lithium Storage in Spheroidal Carbon-Coated Silicon Nanocomposites as Anodes for Lithium-Ion Batteries. *Angew. Chem., Int. Ed.*. **2006**, *45*, 6896−6899.
(57) Gao, B.; Yue, G. Z.; Qiu, Q.; Cheng, Y.; Shimoda, H.; Fleming, L.; Zhou, O. Fabrication and Electron Field Emission Properties of Carbon Nanotube Films by Electrophoretic Deposition. *Adv. Mater.* **2001**, *13*, 1770−1773.
(58) Pascall, A. J.; Sullivan, K. T.; Kuntz, J. D. Morphology of Electrophoretically Deposited Films on Electrode Strips. *J. Phys. Chem. B* **2013**, *117*, 1702−1707.
(59) Zhou, L. J.; Hou, Z. F.; Wu, L. M. First-Principles Study of Lithium Adsorption and Diffusion on Graphene with Point Defects. *J. Phys. Chem. C* **2012**, *116*, 21780−21787.
(60) Tarascon, J. M.; Armand, M. Issues and Challenges Facing Rechargeable Lithium Batteries. *Nature* **2001**, *414*, 359−367.
(61) Xu, K. Nonaqueous Liquid Electrolytes for Lithium-Based Rechargeable Batteries. *Chem. Rev.* **2004**, *104*, 4303−4417.
(62) Liu, N. A.; Hu, L. B.; McDowell, M. T.; Jackson, A.; Cui, Y. Prelithiated Silicon Nanowires as an Anode for Lithium Ion Batteries. *ACS Nano* **2011**, *5*, 6487−6493.

DOI: 10.1021/acsami.5b01315
ACS Appl. Mater. Interfaces 2015, 7, 14201−14210